Chemical Methodologies 6(2022) 1007-1022

Chemical Methodologies

Journal homepage: http://chemmethod.com

Original Research Article

Structural, Characterization, and Biological Activity of Novel Schiff Base Ligand Derived from Pyridoxal with 2-Aminobenzothazol and Its Complexes

Ahmed A. Ismail*, Sajid M. Lateef

Department of Chemistry, College of Education for Pure Science (Ibn Al Haitham), University of Baghdad, Baghdad, Iraq

ARTICLE INFO

Article history

Submitted: 2022-06-13
Revised: 2022-08-22
Accepted: 2022-09-01
Manuscript ID: CHEMM-2208-1600
Checked for Plagiarism: Yes
Language Editor:
Dr. Fatimah Ramezani
Editor who approved publication:
Dr. Lotf Ali Saghatforoush

DOI:10.22034/CHEMM.2022.357804.1600

KEYWORDS

Pyridoxal
2-aminobenzothazol
FT-IR
UV-Vis

ABSTRACT

A [VO(II), Mn(III), Fe(II), Co(II), Ni(II), Cu(II), and Pt(IV)] complexes prepared from 4-((benzo [d] thiazol-2-yl imino) methyl)-5-(hydroxymethyl)-2-methylpyridin 3-ol, ligand (HL^1) Schiff bases is newly synthesized which is derived from the reaction between one equivalent of (pyridoxal hydrochloride) and one equivalent for (2-aminobenzothiazole). Multiple techniques and devices were used to diagnose the prepared compounds. Among these techniques are Melting Point Measurements, Fourier Transform Infrared Spectra, Conductivity Measurements, Electronic spectra UV-Vis., Mass Spectroscopy, Metal Analysis, Elemental Microanalysis, Magnetic Moment Measurement, Thermal Gravimetric Analysis TGA, ^{1}H, and ^{13}C-NMR Spectra. Then, it was measured the biological activity of the prepared compounds against four types of bacteria (*Klebsiella pneumoniae and pseudomonas*) (G-), (*Staphylococcus aureus* and *bacillus subtilis*) (G+), and a one type of fungus (*Candida albicans*).

GRAPHICAL ABSTRACT

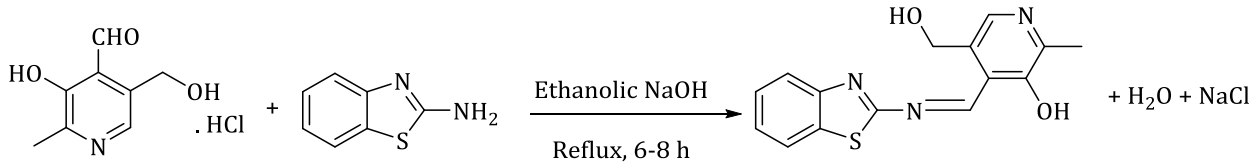

* Corresponding author: Ahmed A. Ismail
✉ E-mail: chem3ps@gmail.com

Introduction

Heterocyclic compounds are cyclic compounds whose rings contain carbon and an additional element, such as oxygen, nitrogen, or sulphur [1]. In organic chemistry, heterocyclic molecules are well-known. They provide various critical physiological tasks in plants and animals, in addition to have significant biological properties, such as penicillin, an antibiotic, and analgesics such as phenobarbital and saccharin, which they classify as heterocyclic compounds [2]. Benzothiazole is a bicyclic heterocyclic compound with a benzene ring fused to a five-membered ring containing nitrogen and sulphur atoms acting as a drug. Benzothiazole-based pharmaceuticals have a wide range of applications [3]. Benzothiazole derivatives are industrially identified as antioxidants [4]. Corrosion inhibitors and surface-active chelating agents for mineral processing [5]. 2-aminobenzothiazoles have a strong reactivity. They are frequently utilized as reactants or reaction intermediates because the NH_2 and end cyclic N functionalities are positioned in such a way that they can react with different bis-electrophilic reagents to generate various fused heterocyclic compounds [6]. In medicine, pyridoxal, one of five naturally interconvertible forms of vitamin B6, has many uses, such as the decarboxylation and transamination of amino acids in the metabolic process [7], its coenzymatic activity in diverse biological processes [8], and its antioxidant capacity [9]. Schiff bases derived from aromatic amines and aldehydes have a broad range of uses in a variety of domains, including biological, inorganic, and analytical chemistry [10]. Numerous novel analytical gadgets demand the presence of organic reagents as critical measurement system components. They are used in different chromatographic methods such as optical and electrochemical sensors, allowing for greater selectivity and sensitivity in detection [11]. The aim of work is to synthesize three novel ligands, two of which are (NNO) type and the other was (NOO) type including Pyridoxal, 2-aminobenzothiazole, 2-amino-4-nitrophenol and 2-amino-6-methoxy benzothiazole. The compounds are characterized by their structures by using melting point and various spectroscopic techniques (FT-IR, UV-Vis, Mass, ^{13}C-NMR, and ^{1}H-NMR), in addition to molar conductance, magnetic susceptibility, elemental microanalysis (C.H.N.S), and thermogravimetric measurements, screening the anti-bacterial activity of the synthesized compounds against four different strains of bacteria (*Klebsiella pneumoniae, pseudomonas, Staphylococcus aureus,* and *Bacillus subtilis*), as well as the anti-fungal activity against one particular type of fungus (*Candida albicans*).

Materials and Methods

Multiple techniques and devices were used to diagnose the prepared compounds. Among these techniques are Melting Point Measurements, Fourier Transform Infrared Spectra with KBr disc in the range of (4000-400 cm^{-1}), Conductivity Measurements at (25 °C) for 10^{-3} $mole.L^{-1}$, Electronic spectra UV.Vis, Mass Spectroscopy, Metal Analysis, Elemental Microanalysis, Magnetic Moment Measurement, Thermal Gravimetric Analysis TGA at a heating rate of 10 ^{o}C/min, ^{1}H, and ^{13}C-NMR spectra. Then, the biological activity of the prepared compounds was measured against four types of bacteria (*Klebsiella pneumoniae* and *pseudomonas*) (G-) and (*Staphylococcus aureus* and *bacillus subtilis*) (G+) and a one type of fungus (*Candida albicans*), as compared with a strong antibiotic (*Ceftriaxone BP*) for bacteria and (*fluconazole*) for fungi.

Synthesis of Schiff base ligand (HL^1)

In an equimolar quantity (1:1) mole ratio, (15 mL) ethanolic solution of pyridoxal hydrochloride (2.03 g, 0.01 mol) was added to the solution of (15 mL) 2-Aminobenzothiazole (0.15 g ,0.01 mol) in the same solvent and they were mixed thoroughly [12]. Next, 0.1% ethanolic NaOH was added to the reaction mixture as a catalyst to adjust pH (pH = 7-8) and the reaction was refluxed with stirring for 6–8 hours. The reaction was monitored by using TLC (Ethylactate/Hexane 3:1). The result was a clear yellow compound, which was dried at room temperature, and then washed with ethanol and recrystallized. Diethyl Ether is used to dry and get a pure sample, as displayed in Scheme 1. Yield=74%, yellowish brown, mp: 112-115 °C, Mw: 299.37 $C_{15}H_{13}N_3O_2S$. The three-dimensional molecular shape of ligand is displayed in Figure 1.

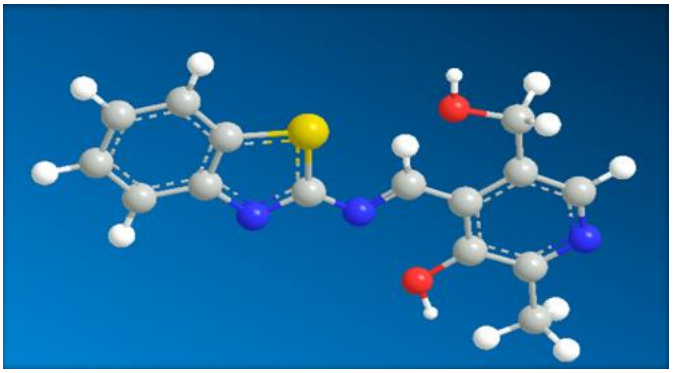

Figure 1: The 3D molecular shape of (HL^1)

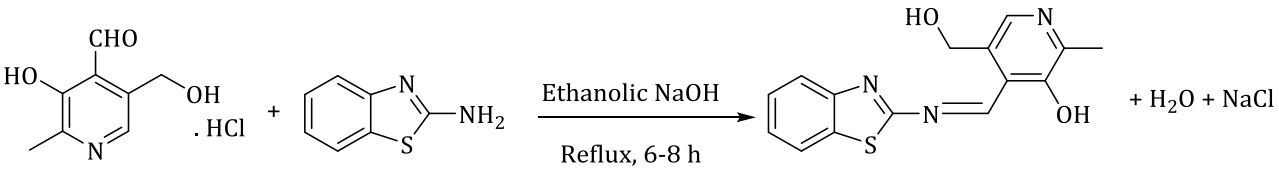

Scheme 1: Synthesis route of the ligand [HL^1]

*Preparation of (HL^1) complexes (**1-7**)*

*Synthesis of $K^+[VO(L^1)(OSO_3)].H_2O$ (**1**)*

A solution of [HL^1] (0.029 g, 1 mmol) was dissolved in (15 mL) ethanol. KOH (1 g/mmol) was added dropwise to a solution, and then this solution was added to a solution of (0.0181 g, 1mmole) of VO(II) sulphate monohydrate dissolved in (10 mL) EtOH. After that,the reaction mixture was allowed to reflux for 3 hours. The precipitate was filtered, washed multiple times with 100% EtOH, and then dried. M.P: (257-259 °C) for the title complex yield (79%), as illustrated in Scheme 2. The physical properties of the complexes and the amount of reactant are demonstrated in Table 1 [13].

*Synthesis of $[Mn(L^1)_2].2H_2O$ (**2**), $[Fe(L^1)_2].H_2O$ (**3**), $[Co(L^1)_2].H_2O$ (**4**),$[Ni(L^1)_2].H_2O$ (**5**), $[Cu(L^1)_2].H_2O$ (**6**) and $[Pt(L^1)_2].Cl_2.H_2O$ (**7**)*

A similar method to that mentioned in synthesizing VO(II) complex was used to synthesize the complexes of [HL^1] with H_2PtCl_6, $MCl_2.nH_2O$ M(II)=[Mn (n=4), Co (n=6), Ni (n=6), Cu (n=2), Fe (n=4), and Pt (n=0)] ions, as displayed in Schemes 3 and 4. Some of the physical properties of complexes and the yield quantities are reported in Table 1.

Results and Discussion

Table 2 lists some physical properties of new ligand and their complexes. The elemental microanalysis (C.H.N.S.) was consistent with the calculated values.

Characterization of ligand HL^1

FT-IR spectra

The spectra were measured by using FT-IR for (HL^1). Figure S1 (Supporting information), shows a new peak at 1627 cm^{-1} related to the stretching frequency of the imine group υ(C=N) [13]. The two peaks at 1377 cm^{-1} and 721 cm^{-1} may be referred to υ(C-N), υ(C-S-C), respectively. The two peaks at 1257 cm^{-1} and 756 cm^{-1} were affiliated to υ(C-O) and δ(C-O), respectively [14].

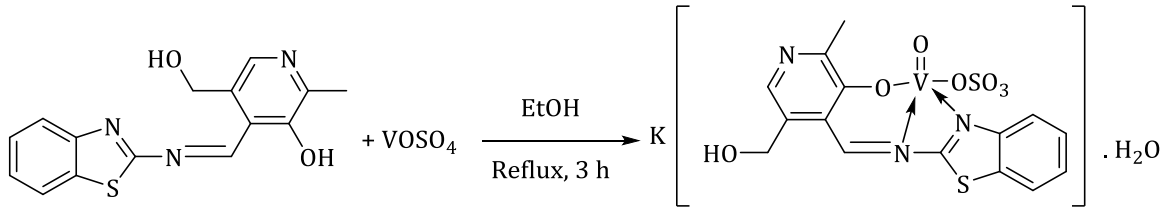

Scheme 2: $K^{+}[VO(L^{1})(OSO_3)].H_2O$ synthesis route

Table 1: Some of the physical properties of the complexes and the yield quantities

Complexes No.	Empirical Formula	Color	M.P °C	Wt. of metal salt (1 mmol)	Yield (%)
1	$K^{+}[VO(L^{1})(OSO_3)].H_2O$	Green	>250	0.0181 g	79
2	$[Mn(L^{1})_2].2H_2O$	Green	130-133	0.0198g	83
3	$[Fe(L^{1})_2].H_2O$	Dark brown	208-210	0.0198 g	76
4	$[Co(L^{1})_2].H_2O$	Yellowish green	>250	0.0237 g	78
5	$[Ni(L^{1})_2].H_2O$	Reddish brown	218-220	0.0237 g	79
6	$[Cu(L^{1})_2].H_2O$	Yellowish green	201-204	0.0170 g	74
7	$[Pt(L^{1})_2].Cl_2.H_2O$	greenish brown	>250	0.040g	73

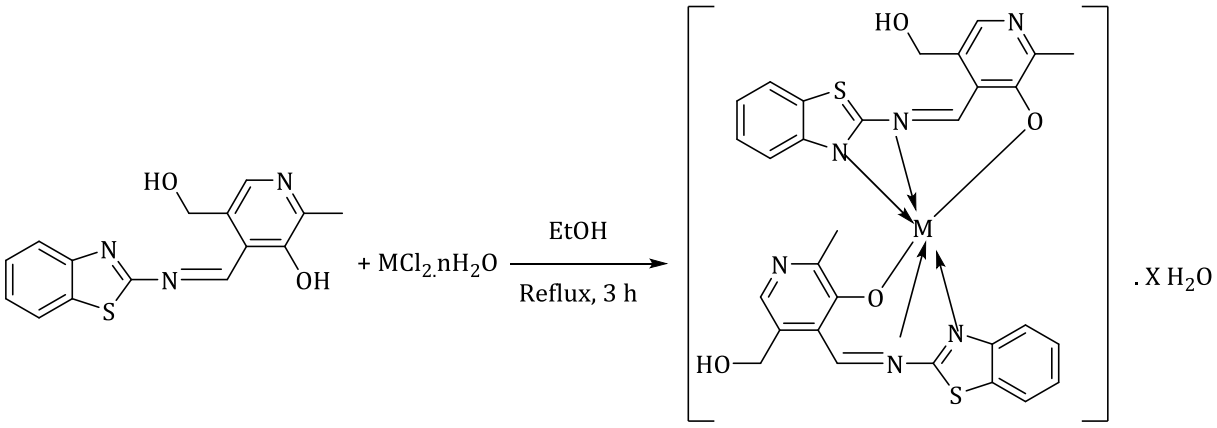

M^{II} = Mn (X=2)
M^{II} = Fe, Co, Ni, Cu (X=1)

Scheme 3: Synthesis route of ligand $[HL^{1}]$ complexes

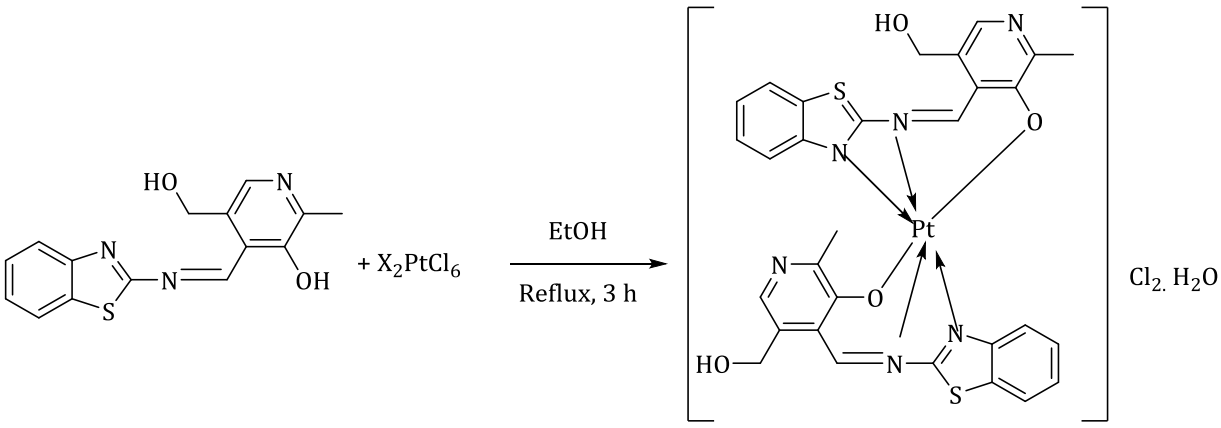

Scheme 4: $[Pt(L^{1})_2].Cl_2.H_2O$ synthesis route

Table 2: Elemental microanalysis results of ligand [HL^1] complexes (**1-7**)

Complexes No.	Compounds	M.wt g/mol	Found / (calc.) %					
			C	H	N	S	metal	K or Cl
1	$K^+[VO(C_{15}H_{12}N_3O_2S)(OSO_3)].H_2O$	518	34.52	2.68	8.07	12.28	9.71	7.44
			34.74	2.70	8.10	12.35	9.84	7.52
2	$[Mn(C_{15}H_{12}N_3O_2S)_2].2H_2O$	687	52.22	4.01	12.15	9.28	7.82	
			52.40	4.07	12.22	9.31	8.00	-
3	$[Fe(C_{15}H_{12}N_3O_2S)_2].H_2O$	670	53.44	3.80	12.48	9.41	8.22	
			53.73	3.88	12.53	9.55	8.32	-
4	$[Co(C_{15}H_{12}N_3O_2S)_2].H_2O$	673	53.38	3.75	12.37	9.43	8.66	
			53.49	3.86	12.48	9.50	8.76	-
5	$[Ni(C_{15}H_{12}N_3O_2S)_2].H_2O$	672.7	53.39	3.76	12.39	9.43	8.50	
			53.61	3.86	12.48	9.51	8.72	-
6	$[Cu(C_{15}H_{12}N_3O_2S)_2].H_2O$	677.5	52.81	3.75	12.21	9.31	9.21	
			53.13	3.83	12.39	9.44	9.37	
7	$[Pt(C_{15}H_{12}N_3O_2S)_2].Cl_2.H_2O$	880	40.78	2.88	9.42	7.16	21.86	7.8
			40.90	2.95	9.54	7.27	22.15	8.04

Calc.: Calculated

Electronic spectra

The electronic spectrum (UV-Vis) was studied for (HL^1). Figure S2 (Supporting information) exhibits four intense absorption peaks at 279 nm, 35842 cm^{-1} and 330 nm, 30303 cm^{-1} affiliated to (л → л*) electronic transition at 348 nm, 28736 cm^{-1} and 400 nm, 2500 cm^{-1} referred to (n→л*) and (LLCT) electronic transition, respectively [14]. The absorption spectral data of (HL^1) ligand are arranged in Table 3.

Table 3: Spectral information of the ligand's [HL^1] electronic data

Ligand	λ (nm)	υ- (cm^{-1})	εmax (molar $^{-1}$ cm^{-1})	Transitions
HL^1	279	35842	1312	л → л*
	330	30303	653	л → л*
	348	28736	657	n→ л*
	400	25000	200	LLCT

^{1}H-NMR spectrum

^{1}H-NMR spectrum for (HL^1) is indicated in Figure S3 (Supporting information). The resonances at chemical shift (δ_H = 7.32–7.51 ppm) are customizable to protons of an aromatic ring (Ar–CH). Mutual coupling causes these protons to appear as a multiple. The signal at (δ_H = 8.44 ppm) was attributed to proton of (N=CH) [15]. The signal at (δ_H = 8.93 ppm) was attributed to the proton of (N–CH) ring. Signal at chemical shift (δ_H =4.96, 4.88 ppm) returns to protons group (CH_2O). The appearance of these protons as a multi-pole is due to the mutual coupling. The signal at (δ_H = 8.20 ppm) was referred to the proton of (C-OH). The spectrum displayed DMSO-related chemical shifts at (δ_H = 2.50 ppm) [16]. The outcomes are presented in Table 4.

^{13}C-NMR spectrum

To analyze ^{13}C-NMR spectrum of (HL^1), Figure S4 (Supporting information) shows chemical shift at range δ= 122.14-141.07 ppm affiliated to the aromatic carbon atoms. The signal at δ=153.95 ppm was directly tied to the (C–N) (C_1), while the chemical shift at (δ=159.88 ppm) was directly tied to the imine carbon atom (C_8). The signal at (δ=197.52ppm) was referred to the (C_9), while the signal at (δ=172.28 ppm) assigned to (C–O–H) (C_{10}), respectively [16]. The signal at (δ=176.22 ppm) was referred to (C– CH_3) (C_{11}), while the signal at (δ=158.55 ppm) was referred to (C–N)

aromatic (C_{12}). The signal at (δ=65.93ppm) was referred to the (CH_2 – OH) (C_{14}), the signal at (δ=13.75ppm) was assigned to methyl group carbon (CH_3) (C_{15}) [17]. The spectrum displayed DMSO-related signal at (δH= 40.47-39.47 ppm) [18]. The results are listed in Table 5.

Table 4: The chemical shift of [HL^1] as measured by ^{1}H-NMR in DMSO-d_6 is denoted in ppm (δ)

Ligand	Functional groups	δ (ppm)
HL^1	N-CH	8.93
	N=CH	8.44
	C-OH	8.20
	Ar-CH	7.32–7.51
	CH_2O	4.96, 4.88
	HDO	3.50
	DMSO	2.50

Table 5: The chemical shift of [HL^1] as measured by ^{13}C-NMR in DMSO-d_6 is denoted in ppm (δ)

Ligand	Functional groups	δ (ppm)
HL^1	C9	197.52
	C11	176.22
	C8	159.88
	C2 – C7	122.14-141.07
	DMSO	40.47 – 39.47
	C15	13.75

Mass spectra

Figure S5 (Supporting information) illustrates the mass spectrum for (HL^1). The ligand's molecular ion peak is observed at m/z^+ = 299.1 [M]·$C_{15}H_{13}N_3O_2S$; requires = 299.07 [19]. The other peaks detected a m/z^+ = 281 correspond to $[C_{15}H_{11}N_3OS]^+$- [H_2O]. The proposed mass fragmentation pattern of (HL^1) can be observed in Scheme 5.

Characterization of complexes

FT-IR spectra

Figure S6 to Figure S12 (Supporting information) show the respective FT-IR spectra of complexes (**1-7**) that were synthesized. The frequencies of characteristic bands are summarized in Table 6. It is expected that a few guiding bands in the ligand spectrum HL^1 will change their position or shape when it is coordinated with a metal ion. The IR spectra of these complexes were compared with those of HL^1 to determine which ligand sites were involved in the chelation process [20]. The band identified at 1627 cm^{-1} corresponds to the stretching frequency of the azomethine (C=N) group of the free ligand (HL^1). This band was shifted to lower or higher frequencies at a range 1604-1647 cm^{-1} in the spectra of all produced complexes.

Electronic spectra

The electronic spectral data of the complexes (**1-7**) were summarized in Table 7 in addition to the electronic transition and proposed geometrical formula. All the electronic spectral data of the complexes (**1-7**) displayed two to three peaks at a wavelength range of (280-390 nm) (35741-25641 cm^{-1}) were found to be attributable to intra-ligand displayed a bathochromic or hypsochromic shift, as compared with (HL^1) free ligand. This verifies that the (HL^1) ligand is coordinated with the central metal ion [21]. Likewise, the spectra of all complexes (**1-7**) illustrated a new intense absorption peak at a range 360-470 nm, 27778-21277 cm^{-1} was attributed to the M→LCT electronic transition [22].

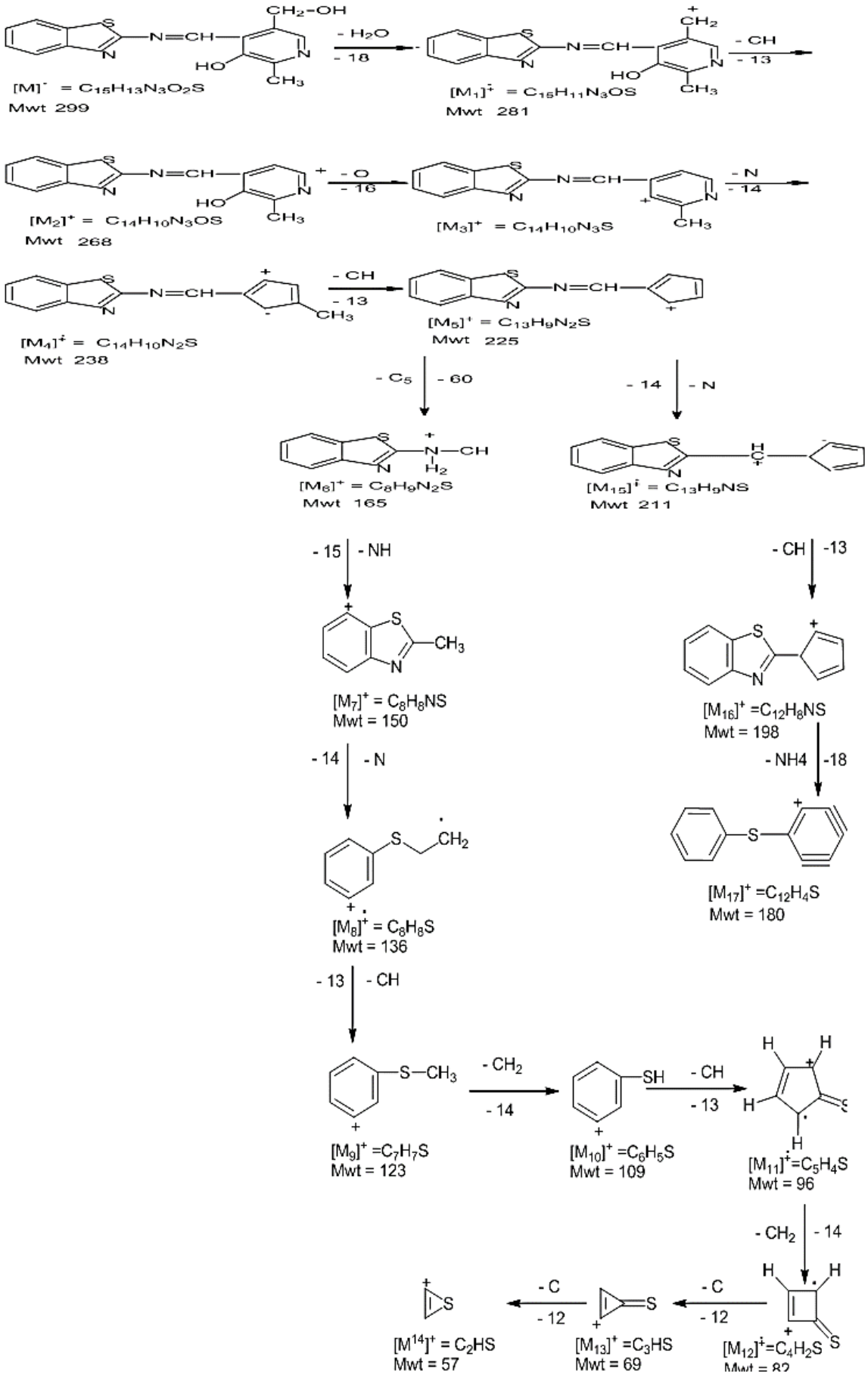

Scheme 5: The suggested mass fragmentation of Schiff base [HL¹]

Molar conductance

It is known that conductivity measurements of the ligand and its complexes are used to determine the conductance of the compounds (electrolyte or nonelectrolyte). Some physical properties and molar conductance values of prepared complexes (**1-7**) were recorded in Table 8 measured in DMSO solvent at 10^{-3} solution at 25 °C [23].

Table 6: Ligand [HL^1] and metal complex FT-IR spectral data (cm^{-1})

No. of complexes	Compounds	υ(O-H)	υ(C-O) δ(C-O)	υ(C=N) imine	υ(C=N) in plane	M - N	M - O
#	HL^1	3059	-	1627	1573	-	-
1	K^+ [$VO(L^1)(OSO_3)$]. H_2O	3330	1261 744	1635	1577	593	470
2	[$Mn(L^1)_2$].$2H_2O$	3336	1261 752	1624	1585	513	486
3	[$Fe(L^1)_2$].H_2O	3332	1265 750	1624	1577	516	452
4	[$Co(L^1)_2$].H_2O	3414	1265 752	1624	1539	559	482
5	[$Ni(L^1)_2$].H_2O	3325	1249 752	1616	1577	574	435
6	[$Cu(L^1)_2$].H_2O	3410	1253 752	1604	1581	578	443
7	[$Pt(L^1)_2$].Cl_2.H_2O	3329	1257 751	1647	1558	578	493

Table 7: Electronic spectral data for [HL^1] complexes

Complexes No.	Compounds	λ (nm)	υ (cm^{-1})	εmax (molar $^{-1}cm^{-1}$)	transitions	Suggested Structure for complexes
#	HL^1	279	35842	1312	л → л*	-
		330	30303	653	л → л*	
		348	28736	657	n→ л*	
		400	25000	200	LLCT	
1	K^+ [$VO(L^1)(OSO_3)$]. H_2O	285	35088	1925	Intra-ligand	Sq.py.
		352	28409	1462	Intra-ligand	
		372	26881	925	MLCT	
		420	23810	80	$^2B_2 \rightarrow {}^2A_1$	
		808	12376	51	$^2B_2 \rightarrow {}^2B_1$	
		906	11038	57	$^2B_2 \rightarrow {}^2E$	
2	[$Mn(L^1)_2$].$2H_2O$	281	35587	627	Intra-ligand	Oh.
		332	30120	513	Intra-ligand	
		348	28736	581	Intra-ligand	
		360	27778	315	MLCT	
		400	25000	206	$^6A_1g \rightarrow {}^4A_1g$, $^4Eg(G)$	
		468	21368	60	$^6A_1g \rightarrow {}^4T_2g$ (G)	
		685	14599	14	$^6A_1g \rightarrow {}^4T_1g$ (G)	
3	[$Fe(L^1)_2$].H_2O	280	35714	1418	Intra-ligand	L.S.Oh.
		350	28571	724	Intra-ligand	
		390	25641	465	Intra-ligand	
		470	21277	124	MLCT	
		716	13966	32	$^1A_1g \rightarrow {}^1T_2g$	
		904	11062	29	$^1A_1g \rightarrow {}^1T_1g$	
		1064	9398	19	$^1A_1g \rightarrow {}^3T_2g$	
4	[$Co(L^1)_2$].H_2O	284	352	1845	Intra-ligand	Oh.
		330	30303	1126	Intra-ligand	
		346	28902	1640	Intra-ligand	

		387	25840	1149	MLCT	
		474	21097	253	$^4T_1g(F) \rightarrow {}^4T_1g$ (P)	
		716	13966	13	$^4T_1g(F) \rightarrow {}^4A_2g(F)$	
		904	11062	21	$^4T_1g(F) \rightarrow {}^4T_2g$ (F)	
5	$[Ni(L^1)_2].H_2O$	291	34364	2264	Intra-ligand	Oh.
		346	28902	1577	Intra-ligand	
		390	25641	896	MLCT	
		450	22222	246	$^3A_2g(F) \rightarrow {}^3T_1g(P)$	
		645	15504	26	$^3A_2g(F) \rightarrow {}^3T_1g(F)$	
		906	11038	18	$^3A_2g(F) \rightarrow {}^3T_2g$ (F)	
6	$[Cu(L^1)_2].H_2O$	284	35211	1890	Intra-ligand	Dist.Oh.
		346	28902	782	Intra-ligand	
		390	25641	493	Intra-ligand	
		436	22936	164	MLCT	
		714	14006	14	$^2B_1g \rightarrow {}^2Eg$	
		800	12500	18	$^2B_1g \rightarrow {}^2B_2g$	
		905	11050	22	$^2B_1g \rightarrow {}^2A_1g$	
7	$[Pt(L^1)_2].Cl_2.H_2O$	291	34364	2257	Intra-ligand	Oh.
		348	28736	1182	Intra-ligand	
		386	25907	614	MLCT	
		415	24096	12	$^1A_1g \rightarrow {}^1T_2g$	

Table 8: Molar conductivity values and some physical properties of HL^1 ligand Complexes (1-7)

Complexes No.	Complexes	M.C S m^2 mol^{-1}	Yield %	m.p. °C	Color	Ratio
1	$K^+[VO(L^1)(OSO_3)].H_2O$	36.81	79	>250	Green	1:1
2	$[Mn(L^1)_2].2H_2O$	8.25	83	130-133	Green	Neutral
3	$[Fe(L^1)_2].H_2O$	13.60	76	208-210	Dark brown	Neutral
4	$[Co(L^1)_2].H_2O$	19.13	78	>250	Greenish yellow	Neutral
5	$[Ni(L^1)_2].H_2O$	20.53	79	218-220	Reddish brown	Neutral
6	$[Cu(L^1)_2].H_2O$	18.24	74	201-204	Greenish yellow	Neutral
7	$[Pt(L^1)_2].Cl_2.H_2O$	78.51	73	>250	Greenish brown	2:1

Magnetic properties

The values of μeff and X_g, X_M, and X_A for the prepared complexes (**1-6**), as presented in Table 9, while Pt(IV) complex is diamagnetic natural.

Thermal analysis

Thermogram of $[Mn(L^1)_2].2H_2O$ is displayed in Figure 2. The recognized peak was found in the TGA curve at 232 °C and was related to the loss of ($2H_2O$, CO) portions, (det. = 0.420 mg, 9.26 %; calc. = 0.501 mg). The second step at 340 °C that designated the loss of (N_2, C_4H_6, CO_2, CO, C_6H_5, and CS_2) fragment, (obs. = 2.027 mg, 44.67%; calc. = 2. 201 mg). The third step at 522 °C is related to the loss of (C_2H_2, CH_4) segments, (obs. = 0.279 mg, 6.15 %; calc. = 0.322 mg). The final remainder of the compound that was observed at a temperature higher than 523ºC is attributed to the ($MnC_{13}H_7N_4$), (det. = 1.812, 39.92 %; calc. = 1.902 mg). The DSC analysis curve verified peaks at 50.3, 175.2, 231.6, 235.5, 415.2, and 520.1 °C refer to an endothermic decomposition process. The exothermic decomposition processes were responsible for the peaks that were observed at 59.1, 180.4, 275.2, 401.7, 424.4, 500.3, and 580.1 °C. The presence of both exothermic and endothermic peaks in an argon atmosphere may indicate that the natural ligand has been ignited. Thus, metal-ligand bond has been broken may be drawn from the final endothermic peak [24, 25].

Table 9: The effective magnetic moment (μeff) values for complexes (**1-6**)

Complexes No.	COMPLEXES	Xg × 10^{-6}	Xm × 10^{-6}	X_A × 10^{-6}	No. of unpaired Electron	μeff	Structure
1	K^+ [VO(L^1)(OSO_3)]. H_2O	2.12	1098.16	1316.69	1	1.77	Sq.Py
2	[Mn(L^1)$_2$].2H_2O	18.41	12647.67	13079.79	5	5.60	Oh.
3	[Fe(L^1)$_2$].H_2O	0.00	0.00	0.00	0	0.00	LS oh
4	[Co(L^1)$_2$].H_2O	14.32	9638.03	10070.15	3	4.19	Oh.
5	[Ni(L^1)$_2$].H_2O	4.321	2846.19	3278.31	2	2.80	Oh.
6	[Cu(L^1)$_2$].H_2O	1.256	850.94	1283.06	1	1.75	Dist.oh

D= - 432.12 x 10^{-6} , Sq.Py = square pyramid , LS = low spin

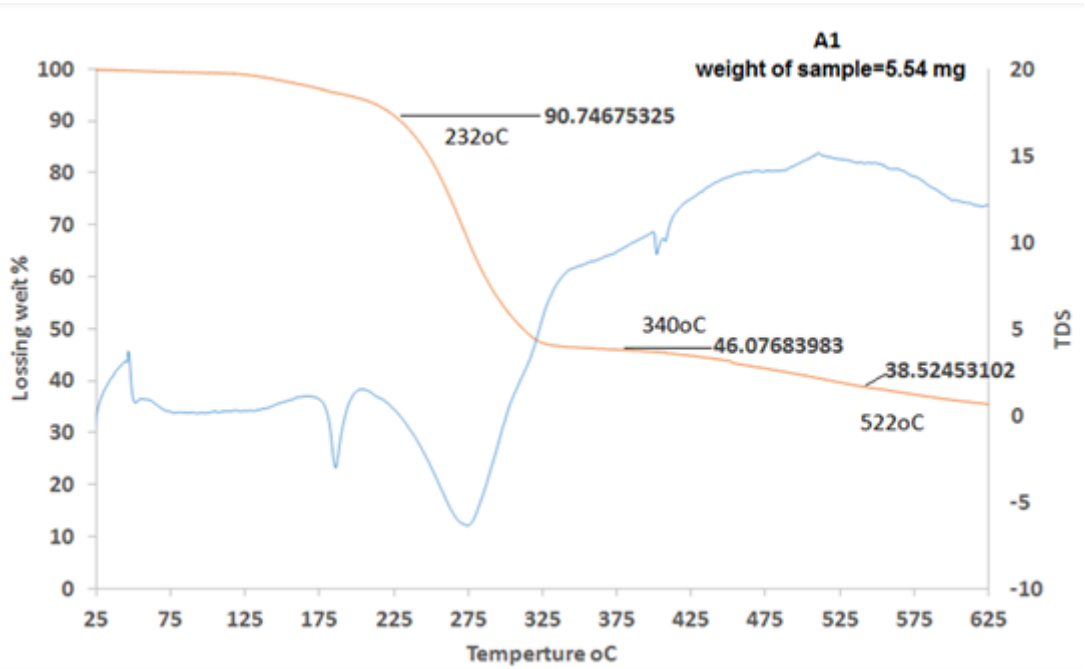

Figure 2: (TGA and DSC) thermogram of [Mn(L^1)$_2$].2H_2O

Biological activity of (HL^1) and its complexes

Antibacterial Activity

The antibacterial activity of the synthesized ligand and its metal complexes was evaluated against four bacterial strains. (*Klebsiella pneumoniae, pseudomonas, Staphylococcus aureus,* and *Bacillus subtilis*). This is to evaluate their potential antibacterial activity by using DMSO as a solvent by the agar well diffusion method, which was considered the zero point of measurement. *Ceftriaxone* was used as a standard drug. Almost all compounds showed good results against all types of bacteria, as indicated in Table 10 and Figures 3, 4, 5, 6, and 7 [26, 27].

Fungi activity

The novel ligand and metal complexes that were synthesized tested on one strain of fungi (*Candida albicans*) so that the final concentration was (0.01) mg/ml, the samples were dissolved in DMSO. Table 10 demonstrates the results of tests on the compounds effects on fungi. Figures 8 and 9 illustrate how well the synthesized compounds stopped the tested fungi's growth [28]. The complexes [Fe(L^1)$_2$].H_2O and [Co(L^1)$_2$].H_2O have a very powerful fungal inhibition impact against the experimental fungal strains [29].

Table 10: Biological activity of the prepared compounds

Compound	Gram Negative (-) *Klebsiella pneumoniae*	Gram Negative (-) *Pseudomonas*	Gram positive (+) *Bacillus subtilis*	Gram positive (+) *Staphylococcus aureus*	Fungi *Candida albicans*
DMSO	0	0	0	0	0
Fluconazole	-	-	-	-	18
Ceftriaxone	7	12	13	12	-
HL^1	12	12	10	12	10
$K^+ [VO(L^1)(OSO_3)]. H_2O$	17	16	15	18	16
$[Mn(L^1)_2].2H_2O$	17	15	15	16	12
$[Fe(L^1)_2].H_2O$	18	19	14	17	20
$[Co(L^1)_2].H_2O$	20	16	13	15	22
$[Ni(L^1)_2].H_2O$	15	16	13	16	13
$[Cu(L^1)_2].H_2O$	15	18	16	14	16
$[Pt(L^1)_2].Cl_2.H_2O$	18	13	13	15	15

Figure 3: The impact of (HL^1) and its complexes on (*BACILLUS SUBTILUS*)

Figure 4: The impact of (HL^1) and its complexes on (*STAPHYLOCOCCUS AUREUS*)

Figure 5: The impact of (HL^1) and its complexes on (*KLEBSIELLA PNEUMONIAE*)

Figure 6: The impact of (HL^1) and its complexes on (*PSEUDOMONAS AERUGINOSA*)

Figure 7: The impact of (HL^1) and its complexes on (*CANDIDA ALBICANS*)

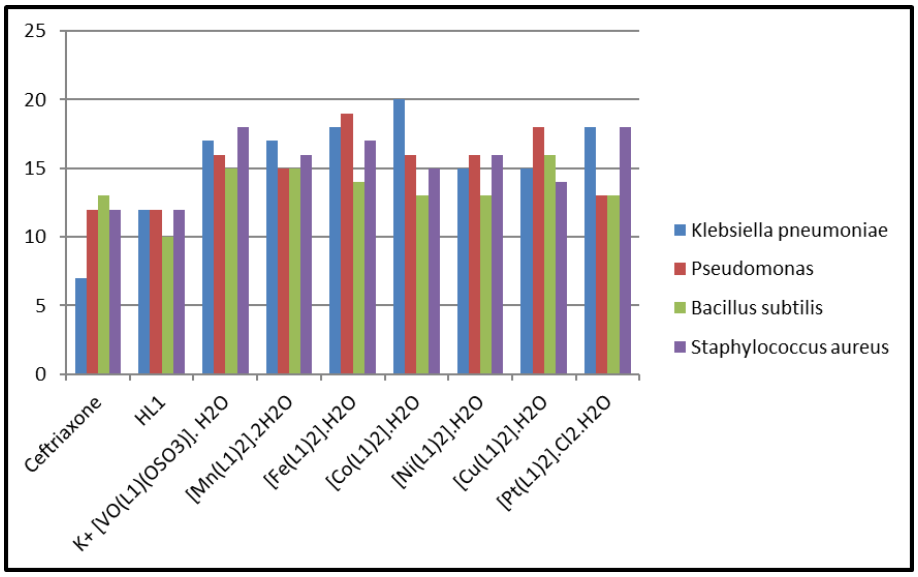

Figure 8: The changes in the diameter (mm) of the zone where (HL^1) and its complexes stop the growth of different types of bacteria

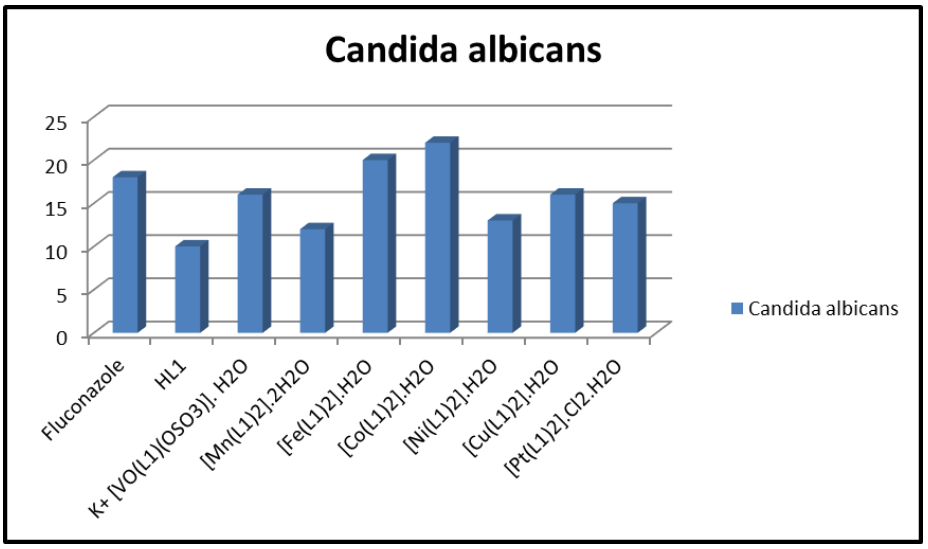

Figure 9: Changes in the diameter (mm) of the zone where (HL1) and its complexes stop the growth of various fungi strains

Conclusion

A novel Ligand (HL^1) was prepared (4-((benzo [*d*] thiazol-2-yl imino)methyl)-5-(hydroxymethyl)-2-methylpyridin 3-ol) which is derived from the Schiff base reaction between (pyridoxal hydrochloride) and (2-Aminobenzothiazole). Then, seven complexes were prepared from (HL^1). All the prepared compounds were characterized by several methods and spectroscopic devices. After that, all of them were tested against the types of bacteria and fungi and the results were very good.

Funding

This research did not receive any specific grant from funding agencies in the public, commercial, or not-for-profit sectors.

Authors' contributions

All authors contributed to data analysis, drafting, and revising of the paper and agreed to be responsible for all the aspects of this work.

Conflict of Interest

There are no conflicts of interest in this study.

ORCID:

Ahmed A. Ismail
https://orcid.org/0000-0002-5963-2681

Supporting Information

Copies of FT-IR, UV-VIs, ^{1}H-NMR, ^{13}C-NMR, Mass spectrum spectra of synthesized complexes. [PDF]

References

[1]. Siddiquee S.,. Recent advancements on the role and analysis of volatile compounds (VOCs) from Trichoderma, In *Biotechnology and Biology of Trichoderma*, 2014, 139-175 [Crossref], [Google Scholar], [Publisher]

[2]. Rossi R.D., What does the acid ionization constant tell you? An organic chemistry student guide, *Journal of Chemical Education*, 2013, **90**:183 [Crossref], [Google Scholar], [Publisher]

[3]. Agarwal S., Gandhi D., Kalal P., Benzothiazole: a versatile and multitargeted pharmacophore in the field of medicinal chemistry, *Letters in Organic Chemistry*, 2017, **14**:729 [Crossref], [Google Scholar], [Publisher]

[4]. Ayodhya D., Veerabhadram G., Facile thermal fabrication of CuO nanoparticles from Cu (II)-Schiff base complexes and its catalytic reduction of 4-nitrophenol, antioxidant, and antimicrobial studies, *Chemical Data Collections*, 2019, **23**:100259 [Crossref], [Google Scholar], [Publisher]

[5]. Suhasaria A., Murmu M., Satpati S., Banerjee P., Sukul D., Bis-benzothiazoles as efficient corrosion inhibitors for mild steel in aqueous HCl: molecular structure-reactivity correlation study, *Journal of Molecular Liquids*, 2020, **313**:113537 [Crossref], [Google Scholar], [Publisher]

[6]. Bhoi M.N., Borad M.A., Panchal N.K., Patel H.D., 2-Aminobenzothiazole containing novel Schiff bases derivatives:Search for new Antibacterial agents, *Journal of Sulfur Chemistry*, 2015, **53**:106 [Crossref], [Google Scholar], [Publisher]

[7]. Mezey R.Ş., Zaharescu T., Lungulescu M.E., Marinescu V., Shova S., Roşu T., Structural characterization and thermal behaviour of some azomethine compounds derived from pyridoxal and 4-aminoantipyrine, *Journal of Thermal Analysis and Calorimetry*, 2016, **126**:1763 [Crossref], [Google Scholar], [Publisher]

[8]. Chumnantana R., Yokochi N., Yagi T., Vitamin B6 compounds prevent the death of yeast cells due to menadione, a reactive oxygen generator, *Biochimica et Biophysica Acta (BBA)-General Subjects*, 2005, **1722**:84 [Crossref], [Google Scholar], [Publisher]

[9]. Mann S., Ploux O., Pyridoxal-5′-phosphate-dependent enzymes involved in biotin biosynthesis: structure, reaction mechanism and inhibition, *Biochimica et Biophysica Acta (BBA)-Proteins and Proteomics*, 2011, **1814**:1459 [Crossref], [Google Scholar], [Publisher]

[10]. Cimerman Z., Miljanić S., Galić N., Schiff bases derived from aminopyridines as spectrofluorimetric analytical reagents, *Croatica Chemica Acta*, 2000, **73**:81 [Google Scholar], [Publisher]

[11]. Abdalrida M.A., Mahdi H.A., Preparation, Identification and Biological Activity of a New Ligand (N, N'-bis (4-Acetamidobenzalidene) 1, 3-diaminopropane) with Some Transition Metal Complexes, *Univesity of Thi-Qar Journal*, 2014, **9** [Google Scholar], [Publisher].

[12]. Anand T., Kumar A.S., Sahoo S.K., A novel Schiff base derivative of pyridoxal for the optical sensing of Zn2+ and cysteine, *Photochemical & Photobiological Sciences*, 2018, **17**:414 [Crossref], [Google Scholar], [Publisher]

[13]. Bhat M., Belagali S.L., Synthesis, In-Vitro and In-Silico Studies of Benzothiazole Azo-Ester Derivatives as Anti-TB Agents. Anti-Infective Agents, 2020, **18**:15 [Crossref], [Google Scholar], [Publisher]

[14]. Nashaan F.A., Al-Rawi M.S., Alhammer A.H., Rabie A.M., Tomma J.H., Synthesis, characterization, and cytotoxic activity of some imides from galloyl hydrazide, *Eurasian Chemical Communications*, 2022, **4**:966 [Crossref], [Google Scholar], [Publisher]

[15]. K Ahmed A., K Jebur I., Ali Muayad Hamzah M., Synthesis, Characterization and Biological Activity Evaluation of Some New Azo Derivatives from 2-Amino Benzothiazole and Their

Derivatives, *Kirkuk University Journal-Scientific Studies*, 2018, **13**:212 [Crossref], [Google Scholar], [Publisher]

[16]. Issa R.M., Khedr A.M., Rizk H., 1H NMR, IR and (UV-Vis) Spectroscopic Studies of Some Schiff Bases Derived from 2-Aminobenzothiazole and 2-Amino-3-Hydroxypyridine, *Journal of the Chinese Chemical Society*, 2008, **55**:875 [Crossref], [Google Scholar], [Publisher]

[17]. AL-Khazraji S.I.C., Ahmed L.M., Synthesis and characterization of some new heterocyclic compounds derived from Thiosemicarbazide, *Chemical Methodologies,* 2022, **6**:157 [Crossref], [Google Scholar], [Publisher]

[18]. Dayan S., Tercan M., Özdemir F.A., Aykutoğlu G., Özdemir N., Şerbetçi Z., Dinçer M., Dayan O., Catalytic and biological activities of homoleptic palladium (II) complexes bearing the 2-aminobenzothiazole moiety, *Polyhedron*, 2021, **199**:115106 [Crossref], [Google Scholar], [Publisher]

[19]. Saipriya D., Prakash A., Kini S.G., Bhatt G.V., Pai K.S.R., Biswas S., Shameer K.M., Design, synthesis, antioxidant and anticancer activity of novel Schiff's bases of 2-amino benzothiazole. *Indian Journal of Pharmaceutical Education and Research*, 2018, **52**:S333 [Crossref], [Google Scholar], [Publisher]

[20]. Ali M.A., Mirza A.H., Nazimuddin M., Dhar P.K., Butcher R.J., Preparation, characterization and antifungal properties of nickel (II) complexes of tridentate ONS ligands derived from N-methyl-S-methyldithiocarbazate and the X-ray crystal structure of the [Ni (ONMeS) CN]·H2O complex, *Transition Metal Chemistry*, 2002, **27**:27 [Crossref], [Google Scholar], [Publisher]

[21]. Cowley A.R., Dilworth J.R., Donnelly P.S., White J.M., Copper complexes of thiosemicarbazone− pyridylhydrazine (THYNIC) hybrid ligands: a new versatile potential bifunctional chelator for copper radiopharmaceuticals, *Inorganic Chemistry*, 2006, **45**:496 [Crossref], [Google Scholar], [Publisher]

[22]. Osowole A.A., Ekennia A.C., Achugbu B.O., Etuk G.H., Synthesis, spectroscopic characterization and structure related antibacterial activities of some metal (II) complexes of substituted triflurobutenol, *Applied Chemistry*, 2013, **59**:15848 [Google Scholar], [Publisher]

[23]. Al-Shammari W.A.M., Lateef S.M., Synthesis, Structural, Thermal and Biological Studies of Ligand Derived from Anthrone with 4-Aminoantipyrine and its Metallic Complexes, *Chemical Methodologies*, 2022, **6**:548 [Crossref], [Google Scholar], [Publisher]

[24]. Sukanya P., Venkata Ramana Reddy C., Synthesis, characterization and in vitro anticancer, DNA binding and cleavage studies of Mn (II), Co (II), Ni (II) and Cu (II) complexes of Schiff base ligand 3-(2-(1-(1H-benzimidazol-2-yl) ethylidene) hydrazinyl) quinoxalin-2 (1H)-one and crystal structure of the ligand, *Applied Organometallic Chemistry*, 2018, **32**:e4526 [Crossref], [Google Scholar], [Publisher]

[25]. Jasim S.A., Riadi Y., Majdi H.S., Altimari U.S., Nanomagnetic macrocyclic Schiff-base–Mn (ii) complex: an efficient heterogeneous catalyst for click approach synthesis of novel β-substitued-1, 2, 3-triazoles, *RSC Advances*, 2022, **12**:17905 [Crossref], [Google Scholar], [Publisher]

[26]. Hassan S.A., Lateef S.M., Majeed I.Y., Structural, Spectral and Thermal studies of new bidentate Schiff base ligand type (NO) derived from Mebendazol and 4-Aminoantipyrine and it's metal complexes and evaluation of their biological activity, *Research Journal of Pharmacy and Technology*, 2020, **13**:3001 [Crossref], [Google Scholar], [Publisher]

[27]. Rabie A.M., Accurate conventional and microwave-assisted synthesis of galloyl hydrazide, *MethodsX*, 2020, **7**:100737 [Crossref], [Google Scholar], [Publisher]

[28]. Abd Al-Mohson Z.M., Synthesis of novel pyrazole derivatives containing tetrahydrocarbazole, antimicrobail evaluation and molecular properties, *Eurasian Chemical Communications*, 2021, **3**:425 [Crossref], [Google Scholar], [Publisher]

[29]. Al Abdeen S.H.Z., Mustafa Y.F., Mutlag S.H., Synthesis of disubstituted anisolodipyrone-derived ester compounds: The search for new bioactive candidates, *Eurasian Chemical Communications*, 2022, **4**:1171 [Crossref], [Google Scholar], [Publisher]

HOW TO CITE THIS ARTICLE
Ahmed A. Ismail, Sajid M. Lateef. Structural, Characterization, and Biological Activity of Novel Schiff Base Ligand Derived from Pyridoxal with 2-Aminobenzothazol and Its Complexes. *Chem. Methodol.*, 2022, 6(12) 1007-1022
https://doi.org/10.22034/CHEMM.2022.357804.1600
URL: http://www.chemmethod.com/article_157242.html